

## Formation of Porous Carbon Materials with in Situ Generated NaF Nanotemplate

Chih-Hao Huang,<sup>†</sup> Yu-Hsu Chang,<sup>†</sup> Hsiao-Wan Wang,<sup>‡</sup> Soofin Cheng,<sup>‡</sup> Chi-Young Lee,<sup>§</sup> and Hsin-Tien Chiu<sup>\*,†</sup>

Department of Applied Chemistry, National Chiao Tung University, Hsinchu, Taiwan, 30050, Republic of China, Department of Chemistry, National Taiwan University, Taipei, Taiwan, 10673, Republic of China, and Materials Science Center, National Tsing Hua University, Hsinchu, Taiwan, 30043, Republic of China

Received: March 27, 2006; In Final Form: April 27, 2006

Porous carbon materials with pore sizes from 3 to 200 nm were synthesized by reacting hexafluorobenzene with Na liquid at 623 K. NaF crystals, a byproduct formed in the reaction, acted as nanotemplate to assist the pore formation. By employing hexafluorobenzene to react with Na incorporated within the channels (diameter 200 nm) of anodized aluminum oxide (AAO) membranes at 323–623 K, the carbon material can be fabricated into aligned porous nanotube arrays (ca. 250 nm in diameter, ca. 20 nm in wall thickness, ca. 0.06 mm in length, and ca. 3–90 nm in pore diameter). These materials were characterized by X-ray diffraction, scanning and transmission electron microscopy, X-ray energy dispersive spectroscopy, electron diffraction, thermal gravimetric analysis, and nitrogen physical adsorption experiments.

## Introduction

Porous materials provide excellent opportunities in numerous technological applications.<sup>1,2</sup> Among different types of porous materials, porous carbon (p-C) has high potential as the component in catalysis, adsorption, sensing, and fuel-cell systems.<sup>3–6</sup> Many types of carbon materials with different pore sizes have been fabricated through replica approaches employing various zeolites or silica as the templates and casts.<sup>7–12</sup> Another frequently used method employs defluorination of PTFE, poly(tetrafluoroethylene), by alkali metals.<sup>13–15</sup> In the present work, we wish to report an efficient new synthesis of p-C by reacting the vapor of C<sub>6</sub>F<sub>6</sub> with Na metal. The growth is an interesting example of a phase separation assisted self-templating process. Moreover, template-assisted growth of carbon nanotubes (CNT) has been demonstrated to be an efficient method to produce aligned arrays of CNT.<sup>16–23</sup> By coupling the reaction between C<sub>6</sub>F<sub>6</sub> and Na with a reactive-template strategy reported before,<sup>24</sup> which employs anodic aluminum oxide (AAO) membrane filled with Na metal as an active cast, arrays of porous CNT (p-CNT) can be fabricated.

## Experimental Section

**Synthesis of p-C.** Na metal was prepared by pyrolyzing NaH (0.15 g, 6.3 mmol, Aldrich) under Ar atmosphere on a silica boat inside a tube furnace at 623 K for 1 h. To the as-formed Na metal at 623 K, C<sub>6</sub>F<sub>6</sub> (99%, Aldrich) vaporized at 298 K was introduced by bubbling under a constant flow of Ar (5 sccm) for 4 h. The as-prepared black product was further washed in refluxing distilled water (300 mL) overnight. The solid product was collected, rinsed with distilled water, and dried at 373 K in air.

**Synthesis of p-CNT.** Na@AAO was prepared by pyrolyzing NaH (0.15 g, 6.3 mmol, Aldrich) on AAO (Whatman Anodisc 13, pore diameter of 200 nm, thickness of 60 μm) at 623 K for 1 h under an Ar atmosphere.<sup>24</sup> The as-prepared Na@AAO was reacted with C<sub>6</sub>F<sub>6</sub> (99%, Aldrich), maintained at 298 K, and

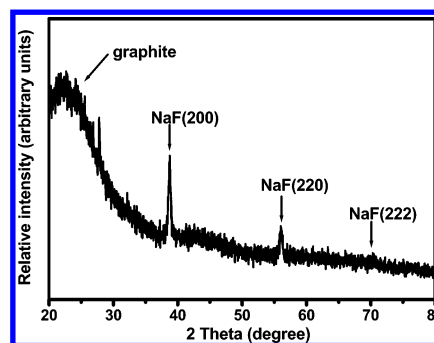


Figure 1. XRD of an as-formed raw product prepared at 623 K.

bubbled with the assistance of a constant flow of Ar (5 sccm) at 323 and 623 K for 4 h to generate black products. The as-prepared products were further washed in refluxing distilled water (300 mL) overnight. Then, the AAO was removed by immersion in 48% HF at room temperature for 9 h. Finally, the products were filtered, rinsed with distilled water, and dried at 373 K in air.

**Characterization of p-C Materials.** A scanning electron microscope (JEOL JSM-6330F at 15 kV and HITACHI S-4000 at 25 kV) and a high-resolution transmission electron microscope (JEOL JEM-4000 at 400 kV) were used to observe the sample morphology. X-ray energy dispersive spectroscopy was used to confirm the element composition of the samples. Crystallinity of the samples was investigated by an X-ray diffractometer (BRUKER AXS D8 ADVANCE, Cu K $\alpha$  radiation, 40 kV and 40 mA). A physical adsorption instrument (Micromeritics ASAP 2010, at 77 K with N<sub>2</sub> gas) was used to investigate surface area and pore size distribution of the samples. Thermal gravimetric analysis (TGA) was carried out on a Pyris Diamond TG/DTA instrument (heating rate of 5 deg/min from room temperature to 900 °C, air flow rate at 100 mL/min).

## Results

**Preparation and Characterization of p-C.** In general, via a Wurtz-type coupling reaction,<sup>25</sup> the vapor of C<sub>6</sub>F<sub>6</sub> was reacted with Na metal, prepared by pyrolyzing NaH under Ar, at 623

\* Address correspondence to this author. E-mail: htchiu@cc.nctu.edu.tw.

<sup>†</sup> National Chiao Tung University.

<sup>‡</sup> National Taiwan University.

<sup>§</sup> National Tsing Hua University.

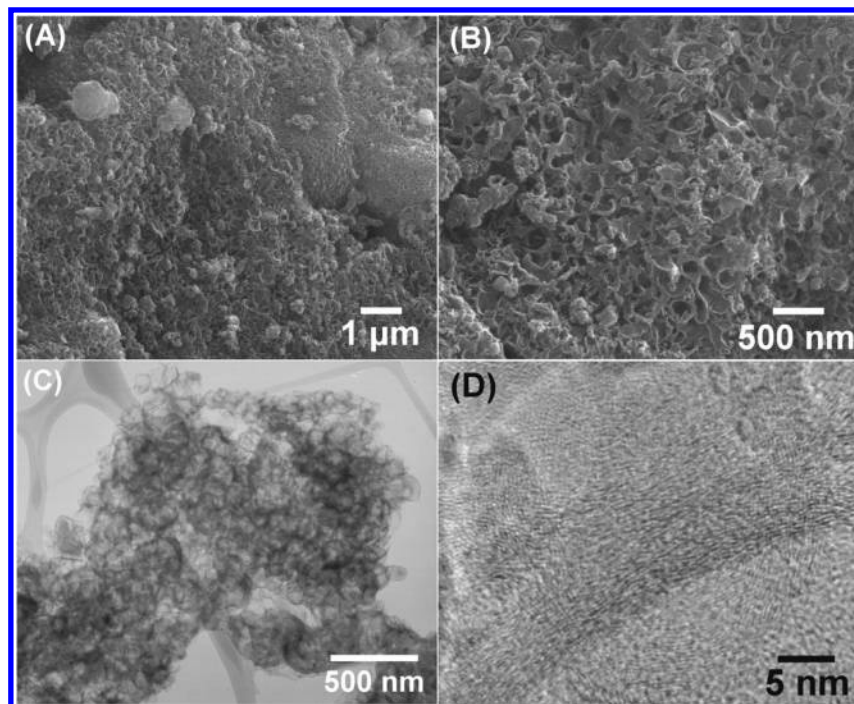


**Figure 2.** Images of p-C prepared at 623 K: (A) low and (B) high magnification SEM and (C) low- magnification and (D) high-resolution TEM.

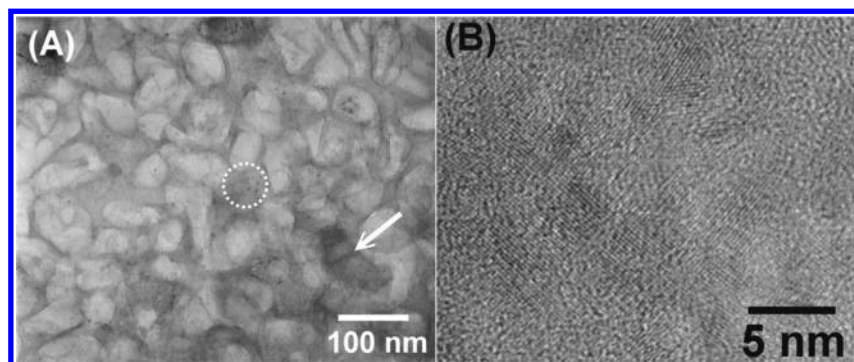


**Figure 3.** TEM images of phase separated p-C and NaF: (A) low magnification image showing NaF crystals pointed out by the arrow and (B) high-resolution image of NaF nanocrystals selected from the circled area in part A.

K for 1 h to offer a dark solid product. As described in the next section, the reaction can be performed at a temperature as low as 323 K. As shown in Figure 1, X-ray diffraction (XRD) of the solid produced at 623 K displays a diffraction pattern that is composed of a broad (002) reflection from graphite (JCPDS 23-0064) and (200), (220), and (222) reflections from NaF (JCPDS 36-1455). No other significant structural information was observed. After the sample was washed with distilled water, the salt was removed and the black solid product was collected. Figure 2A is a typical scanning electron microscopic (SEM) image of the isolated material. In the enlarged image, Figure 2B, morphology of the material is shown to have innumerable pores with diameters less than 200 nm. X-ray energy dispersive spectroscopy (EDX) confirms that the solid is composed of carbon while the concentrations of sodium and fluorine are below the detection limits. A low-magnification transmission electron microscopic (TEM) image in Figure 2C also shows the porous nature of the solid product, with pore diameters less than 200 nm. In a high-resolution transmission electron microscopic (HRTEM) image (Figure 2D) of the sample, the presence of fringes spaced ca. 0.35 nm apart is observed. Since the fringes are not well ordered, we suggest that the edges of the p-C have a short-range ordering of graphite texture. The thickness of the p-C wall, deduced from the image, is 3–15 nm. Occasionally,

NaF nanoparticles can be observed inside p-C by TEM. For example, at point indicated by the arrow in Figure 3A, the presence of a NaF crystal ca. 80 nm in size is identified by EDX. In addition, from the circled area in Figure 3A, several minute nanocrystals with sizes of 2–4 nm are observed by HRTEM, as shown in Figure 3B. The lattice fringes are spaced 0.23 nm apart, which coincides well with the {200} interplanar distance of NaF (JCPDS 36-1455). This confirms that the nanosized NaF crystals acted as the templates for the formation of the porous structure.

**Preparation and Characterization of p-CNT.** Previously, we demonstrated that by pyrolyzing NaH on top of AAO membranes, the as-formed Na flowed into the channels of AAO and produced reactive templates Na@AAO.<sup>24</sup> By reacting Na@AAO with C<sub>6</sub>Cl<sub>6</sub>, amorphous carbon nanotubes were fabricated inside the AAO cast. On the basis of the product morphology, we concluded that metallic Na existed as nanotubes inside the AAO channels of Na@AAO. We extend the strategy in this study. By employing C<sub>6</sub>F<sub>6</sub> to react with Na@AAO at 323 and 623 K, black products were insolated. After the AAO template and the salt were removed, the products were investigated by electron microscopy. A low-magnification SEM image of the product prepared at 323 K after the AAO cast was removed is shown in Figure 4A. It displays that the sample

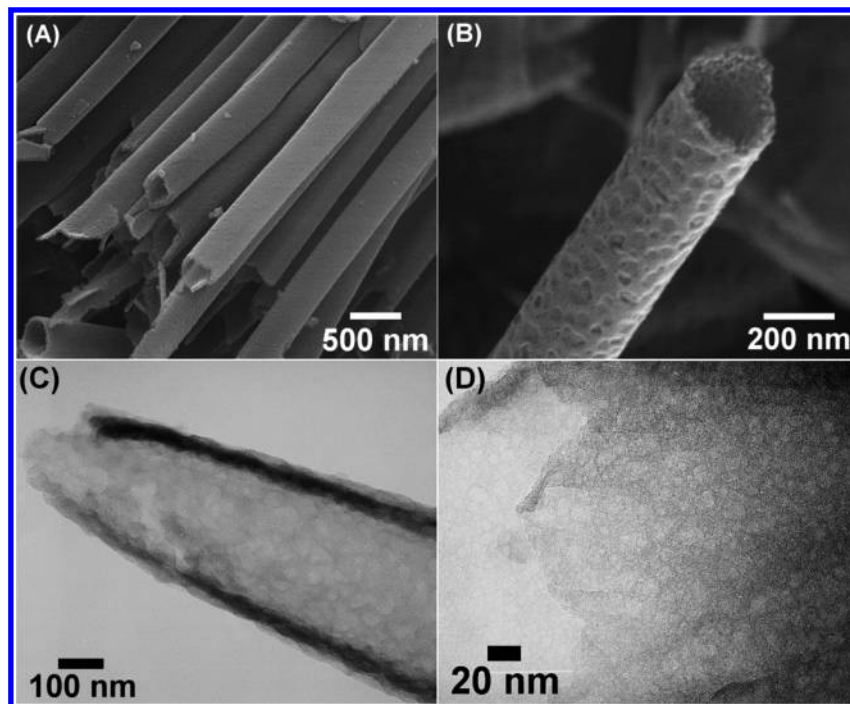


**Figure 4.** Images of p-CNT prepared at 323 K: (A) low and (B) high magnification SEM and (C) low- and (D) high-magnification TEM.

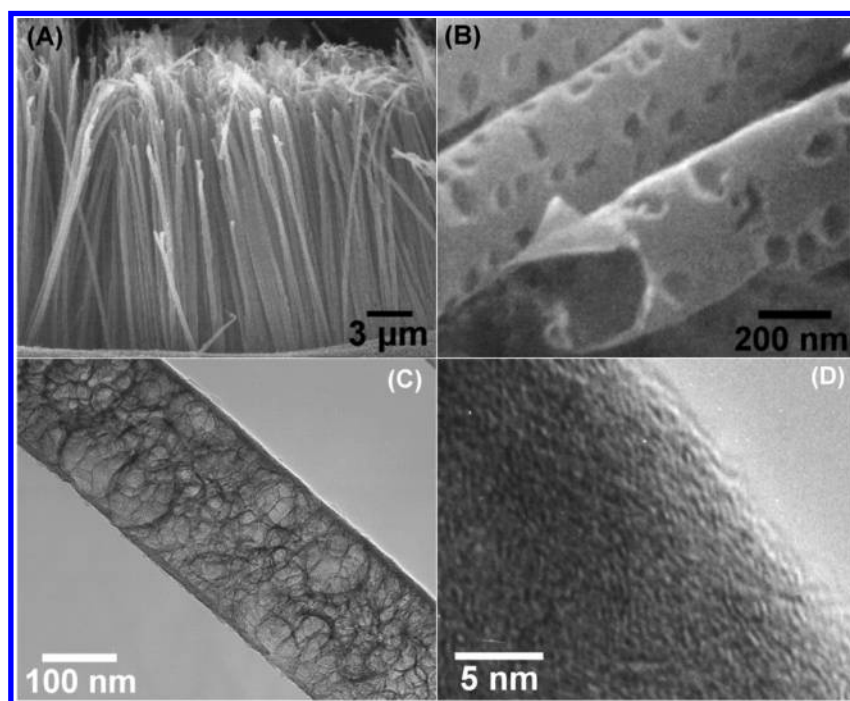


**Figure 5.** Images of p-CNT prepared at 623 K: (A) low and (B) high magnification SEM and (C) low- and (D) high-resolution TEM.

is an aligned array of nanotubes with diameters of 200–250 nm. This is close to the channel diameter of the AAO template. An EDS study confirms that the material is composed of carbon. From other SEM images, the length of the nanotubes is estimated to be 60  $\mu\text{m}$ , which is close to the thickness of the AAO membrane. Figure 4B shows an enlarged SEM image of a p-CNT with undulate inner and outer surfaces. On the basis of the results discussed in the previous section, the unevenness of the surfaces is attributed to the presence of pores generated by the byproduct NaF. A TEM image (Figure 4C) of a tube also shows an average diameter of 220 nm, which is comparable to the SEM observation. In Figure 4D, an HRTEM image shows the detailed microstructure of a p-CNT. It reveals a wall thickness of ca. 15–20 nm and numerous pores of several

nanometers inside the wall. Thus, we successfully fabricated, via a simple process, a new type of p-CNT from this unique self-templating and casting approach.

From SEM images and EDX studies, the sample prepared at 623 K is also identified to be an aligned array of p-CNT (lengths of ca. 60  $\mu\text{m}$ , diameters of ca. 200–300 nm, and pore sizes of ca. 20–100 nm). Examples of low- and high-magnification images are shown in Figure 5, panels A and B, respectively. In Figure 5C, a TEM image of an individual p-CNT shows the presence of innumerable pores of 15–90 nm in the wall, which correlates well with the SEM observation. An HRTEM image (Figure 5D), selected from the edge of the p-CNT shown in Figure 5C, displays textured graphene layers. The overall pore structure in p-CNT is nearly identical with that of p-C discussed

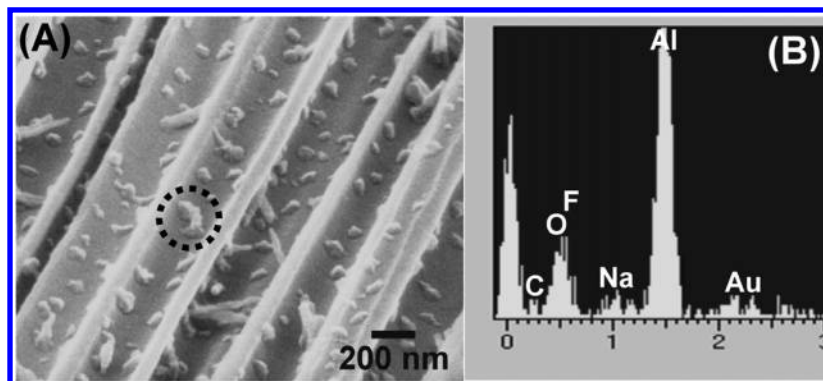


**Figure 6.** (A) Cross sectional SEM image of AAO after removal of p-CNT prepared at 623 K showing crystals in the channels and (B) EDS from the circled area in part A.

above. A TGA result showed that a p-CNT sample, annealed at 1173 K under vacuum followed by removing the AAO template, was oxidized in air at 710 K. The sharp weight loss suggests that the sample contained less ordered carbon structure.<sup>26</sup> The process removed ca. 63% weight of the material in the sample. The residue, which was stable up to 1173 K, is assigned to unremoved NaF byproduct.

The following observations further support the role of the NaF byproduct as an in situ generated nanotemplate for pore formation. Figure 6A shows an enlarged cross-sectional SEM view of an AAO membrane after p-CNT formed at 623 K was removed from the cast. On the exposed channel surface, solid islands with sizes of several tens of nanometers are observed. An EDX study (Figure 6B) of an island, selected from the circled area in Figure 6A, reveals the presence of Na and F. Consequently, the islands are identified to be NaF crystals. The crystal size and shape are in good agreement with the pore structures observed in Figure 5B,C. Thus, we conclude that the NaF nanocrystals and the AAO membrane acted as the cast to influence the p-CNT structure cooperatively. The NaF worked as the in situ generated nanotemplate, which assisted the pore formation, while the AAO membrane performed the role of the cast, which aided the tubular shape development.

**BET Analysis of p-C Materials Prepared at 623 K.** From the SEM and TEM studies discussed above, the carbon materials possessed pores with sizes ranging from several to several tens of nanometers. Typical nitrogen adsorption–desorption isotherms of p-C and p-CNT prepared at 623 K are shown in Figure 7, panels A and B, respectively. In the region of middle and high  $P/P_0$ , the amount of  $N_2$  adsorption increases sharply. The phenomenon, a steep increase in the isotherm at high pressures ( $P/P_0 \rightarrow 1$ ), confirms that large macropores are present in the materials. In addition, large hystereses are observed in Figure 7. This is evidence for a network pore system with distinct polydispersity in size.<sup>27,28</sup> The observation is in good agreement with the TEM images in Figures 2C and 5C. Estimated from Figure 7A, the Brunauer–Emmett–Teller (BET) surface area is  $161 \text{ m}^2 \text{ g}^{-1}$ . By using Barret–Joyner–Halenda (BJH) method, the smallest pore size in p-C can be calculated from the desorption branch of the nitrogen isotherm. The reason the desorption branches, instead of the adsorption ones, were used is explained below. According to the Kelvin equation,<sup>27</sup> the desorption branch of the isotherms is usually more reasonable to derive the diameters of cylindrical pores when the contact angle between the adsorbate, which was nitrogen in this study, and the pore wall is assumed to be zero. Nevertheless, the huge hysteresis loops of the isotherms of p-C and p-CNT materials indicate the pores could probably be described by an ink-bottle model.<sup>27</sup> The rapid increase in adsorption volume in the

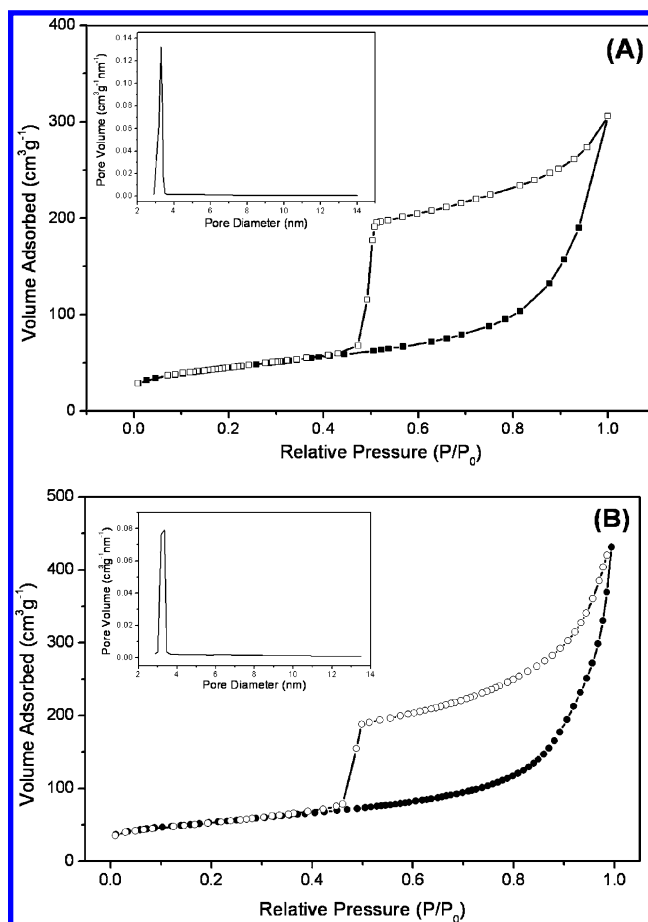
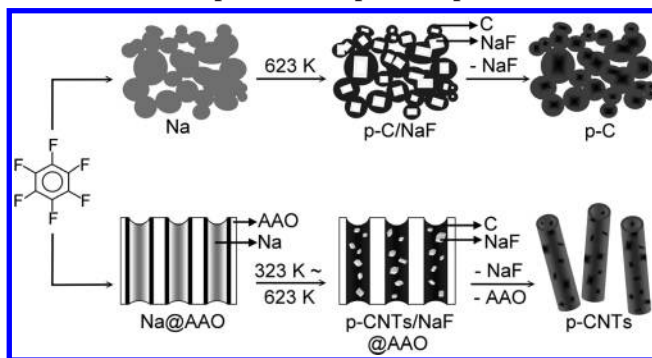


**Figure 7.** Nitrogen adsorption–desorption isotherms and BJH pore size distribution from the desorption branches (insets): (A) p-C (■: adsorption branch; □: desorption branch) and (B) p-CNT (●: adsorption branch; ○: desorption branch).

adsorption branches at higher  $P/P_0$  was related to the large diameter of the bottle shaped pores, while that in the desorption branches at lower  $P/P_0$  was correlated to the smaller diameter of the neck. Thus, the pores of this region are estimated to be as small as 3–3.5 nm. This agrees with the mesopores (sizes 2–4 nm) observed in Figure 3B, which formed after the NaF nanocrystals in the carbon matrix were removed. This is comparable to a previous study in which removal of fluorides from a carbon matrix by acid treatment was found to leave empty sites as pores.<sup>29</sup> The BET surface area estimated from Figure 7B is  $183 \text{ m}^2 \text{ g}^{-1}$ . The calculated pore size distribution from the desorption branch, using the BJH method, also displays that the pores exhibit a size limit at 3–3.5 nm. These

## SCHEME 1: Preparations of p-C and p-CNT



experimental data are comparable to the values reported recently in another study.<sup>11</sup>

### Discussion

For summary, a scheme for the formation of p-C materials by reacting  $C_6F_6$  with Na and Na@AAO is shown in Scheme 1. The process utilized the strong reducing capability of metallic Na to remove F atoms from  $C_6F_6$  and facilitated the solid carbon formation via a Wurtz-type coupling reaction. As shown in the TEM images in Figure 3, due to phase separation, the NaF byproducts of various sizes are incorporated within the carbon solid. This assists the formation of the macro- and mesoporous structures. Another possible origin of the mesopores, as suggested in the literature, is from the disordered stacking of graphene sheets shown in Figures 2D and 5D.<sup>30</sup> The p-CNT prepared from  $C_6F_6$  in this study shows significant structural difference from the CNT, which had smooth nonporous walls, synthesized from  $C_6Cl_6$  previously.<sup>24</sup> The origin of this is proposed to be the difference in physical properties of the byproduct salts NaF and NaCl. This includes the melting point and the energy of formation, which would affect the crystal sizes and their affinity to surroundings. In this study, as shown in Figures 3 and 6, we find that NaF adhere better to the AAO template and the as-formed carbon solid.<sup>31</sup> This was not observed in the previous investigation employing  $C_6Cl_6$  as the source of carbon.<sup>24</sup>

It is striking to discover that p-CNT can be formed at a temperature as low as 323 K. This observation may be attributed to the high energy of formation of NaF and the highly exothermic reaction.<sup>31</sup> The reaction rate probably is accelerated significantly within nanoscopic zones where the reaction between gaseous  $C_6F_6$  molecules and Na releases enough energy to overcome the overall reaction barrier.

### Conclusions

By employing  $C_6F_6$  to react with Na, a unique type of p-C material was formed. The self-generated NaF acted as the nanotemplate to shape the carbon material into the observed porous structure. By using the reactive template Na@AAO, the p-C can be fabricated further into nanotubes with a structure significantly different from the Iijima type CNT.<sup>32,33</sup> The process reported here is relatively low temperature and does not require plasma, autoclave, and catalyst assistance. We anticipate these new materials to be useful in many applications. For example, a preliminary investigation showed that p-CNT retained essential nanostructural features after being graphitized at 3073 K. We expect polymer chains could entangle this unique carbon

material effectively by passing through the porous structure.<sup>34,35</sup> This may offer a new type of low-density and high-strength composite material. Investigation is in progress.

**Acknowledgment.** This work was supported by the National Science Council of Taiwan, Republic of China.

**Supporting Information Available:** XRD pattern of as-formed p-C raw product and TGA of p-CNT. This material is available free of charge via the Internet at <http://pubs.acs.org>.

### References and Notes

- (1) Ying, J. Y.; Mehnert, C. P.; Wong, M. S. *Angew. Chem., Int. Ed. Engl.* **1999**, *38*, 56.
- (2) Schüth, F. *Angew. Chem., Int. Ed.* **2003**, *42*, 3604.
- (3) Che, G.; Lakshmi, B. B.; Fisher, E. R.; Martin, C. R. *Nature* **1998**, *393*, 346.
- (4) Joo, S. H.; Choi, S. J.; Oh, I.; Kwak, J.; Liu, Z.; Terasaki, O.; Ryoo, R. *Nature* **2001**, *412*, 169.
- (5) Dalton, A. B.; Collins, S.; Munoz, E.; Razal, J. M.; Ebron, V. H.; Ferratis, J. P.; Coleman, J. N.; Kim, B. G.; Baughman, R. H. *Nature* **2003**, *423*, 703.
- (6) Sakintuna, B.; Yurum, Y. *Ind. Eng. Chem. Res.* **2005**, *44*, 2893.
- (7) Kyotani, T.; Nagai, T.; Inoue, S.; Tomita, A. *Chem. Mater.* **1997**, *9*, 609.
- (8) Johnson, S. A.; Brigham, E. S.; Ollivier, P. J.; Mallouk, T. E. *Chem. Mater.* **1997**, *9*, 2448.
- (9) Lee, J.; Yoon, S.; Hyeon, T.; Oh, S. M.; Kim, K. B. *Chem. Commun.* **1999**, 2177.
- (10) Ryoo, R.; Joo, S. H.; Kruk, M.; Jaroniec, M. *Adv. Mater.* **2001**, *13*, 677.
- (11) Kim, M.; Sohn, K.; Kim, J.; Hyeon, T. *Chem. Commun.* **2003**, 652.
- (12) Han, B. H.; Zhou, W.; Sayari, A. *J. Am. Chem. Soc.* **2003**, *125*, 3444.
- (13) Tanaike, O.; Hatori, H.; Yamada, Y.; Shiraiishi, S.; Oya, A. *Carbon* **2003**, *41*, 1759.
- (14) Tanaike, O.; Yoshizawa, N.; Hatori, H.; Yamada, Y.; Shiraiishi, S.; Oya, A. *Carbon* **2002**, *40*, 457.
- (15) Hlavaty, J.; Havan, L. *Carbon* **1999**, *37*, 1029.
- (16) Miao, J. Y.; Cai, Y.; Chan, Y. F.; Sheng, P.; Wang, N. *J. Phys. Chem. B* **2006**, *110*, 2080.
- (17) Sui, Y. C.; Acosta, D. R.; Gonzalez-Leon, J. A.; Bermudez, A.; Feuchtwangler, J.; Cui, B. Z.; Flores, J. O.; Saniger, J. M. *J. Phys. Chem. B* **2001**, *105*, 1523.
- (18) Rajesh, B.; Thampi, K. R.; Bonard, J. M.; Xanthopoulos, N.; Mathieu, H. J.; Viswanathan, B. *J. Phys. Chem. B* **2003**, *107*, 2701.
- (19) Che, G.; Lakshmi, B. B.; Martin, C. R.; Rodney, R. S.; Fisher, E. R. *Chem. Mater.* **1998**, *10*, 260.
- (20) Miller, S. A.; Young, V. Y.; Martin, C. R. *J. Am. Chem. Soc.* **2001**, *123*, 12335.
- (21) Lee, J. S.; Gu, G. H.; Kim, H.; Jeong, K. S.; Bae, J.; Suh, J. S. *Chem. Mater.* **2001**, *13*, 2387.
- (22) Jeong, S. H.; Lee, O. J.; Oh, S. H.; Park, C. G.; Lee, K. H. *Chem. Mater.* **2002**, *14*, 1859.
- (23) Yang, Q.; Xu, W.; Tomita, A.; Kyotani, T. *J. Am. Chem. Soc.* **2005**, *127*, 8956.
- (24) Wang, L. S.; Lee, C. Y.; Chiu, H. T. *Chem. Commun.* **2003**, 1964.
- (25) Peter, K.; Vollhardt, C.; Schore, N. E. *Organic Chemistry*, 3rd ed.; Freeman Press: New York, 1998; pp 325–326.
- (26) Mckee, G. S. B.; Vecchio, K. S. *J. Phys. Chem. B* **2006**, *110*, 1179.
- (27) Gregg, S. J.; Sing, K. S. W. *Adsorption, Surface Area, and Porosity*; Academic Press: London, UK, 1982; Chapter 3.
- (28) Polarz, S.; Smarsly, B.; Schattka, J. H. *Chem. Mater.* **2002**, *14*, 2940.
- (29) Shiraiishi, S.; Kurihara, H.; Tsubota, H.; Oya, A.; Soneda, Y.; Yamada, Y. *Electrochem. Solid-State Lett.* **2001**, *4*, A5.
- (30) Foley, H. C. *Microporous Mater.* **1995**, *4*, 407.
- (31) Weast, R. C. *CRC Handbook of Chemistry and Physics*, 1st Student ed.; CRC Press: Boca Raton FL, 1988.
- (32) Iijima, S. *Nature* **1991**, *354*, 56.
- (33) Iijima, S.; Ichihashi, T. *Nature* **1993**, *363*, 603.
- (34) Ge, J. J.; Hou, H.; Li, Q.; Graham, M. J.; Greiner, A.; Reneker, D. H.; Harris, F. W.; Cheng, S. Z. D. *J. Am. Chem. Soc.* **2004**, *126*, 15754.
- (35) Zhang, W. D.; Shen, L.; Phang, I. Y.; Liu, T. *Macromolecules* **2004**, *37*, 256.